ADVANCED MATERIALS INTERFACES
www.advmatinterfaces.de

In Situ Raman Observation of Dynamically Structural Transformation Induced by Electrochemical Lithium Intercalation and Deintercalation from Multi-Electrochromic V_2O_5 Thin Films

Zhuohui Zhang, Weiping Xie, Jia Li, Hongliang Zhang, Qiang Wang, Chengli Zhang, Guanglong Xu, Junhua Gao, A. A. Rogachev, and Hongtao Cao**

Understanding the dynamic nature of electrochemical interface induced by ion transfer is of great significance. Herein, in situ Raman spectroscopy combined with electrochemistry has been developed to real-time monitor the transfer of lithium ions at electrode-electrolyte interface and reveal the associated structure and performance variation of the vanadium pentoxide (V_2O_5) thin films on the indium tin oxide/silver/aluminum zinc oxide/poly(ethylene terephthalate) (ITO/Ag/AZO/PET) substrates. It is demonstrated that the Raman active/silent states of the vibrational modes of V—O, V_3—O, and V—O bonds, as well as the transformation of the V_2O_5 thin films from V_2O_5 to lithium vanadate ($Li_xV_2O_5$), can be reversibly changed with reversible extraction/insertion of lithium ions. In situ UV-vis spectroscopy in combination with in situ Raman analysis is applied to show that the reversible evolutions involving $V_2O_5/Li_xV_2O_5$ and VO bonding characteristic contribute to the multi-color electrochromic characteristic of the V_2O_5 thin films enabling a superior optical modulation of up to 75.41%. This experimental approach establishes a significative guideline for the more elaborate research on the dynamic nature of electrochemical interface.

1. Introduction

The electrochromic materials, whose optical properties (transmittance, reflectance, and absorbance) reversibly change with transitions in polarity and intensity of an applied electric field,[1] show increasingly broad prospects due to their huge commercial application potential in the fields of variable reflection mirrors, smart windows, displays, flexible wearable fabric and so on.[2–4] As the promising electrochromic material that can display both cathodic and anodic coloration, vanadium pentoxide (V_2O_5) has received tremendous research attention owing to its layered structure and several oxidation states (V^{2+} to V^{5+}).[5,6] Both amorphous and crystalline layered V_2O_5 thin films enable reversibly electrochemical conduction cations intercalation and deintercalation enjoy multi-electrochromic performance,[5,7] accompanying a reversible redox reaction from V_2O_5 to $M_xV_2O_5$ (M = Li, Na, Zn).[1,8,9] For instance, the nanocrystal-in-glass (nanocrystals embedded amorphous matrix) V_2O_5 thin films with large interlayer spacing can withstand stress caused by intercalation/deintercalation of conduction ions into/from the host structure, thereby avoiding the collapse of the host structure of the film and realizing the reversible insertion of lithium ions.[8,10] The interface between the V_2O_5 thin films and electrolytes has been shown to be crucial in determining the electrochemical and electrochromic properties. While ex situ methods have yielded a great deal of information for understanding electrochemical lithium intercalation and deintercalation processes,[11–13] the operation dynamics of the V_2O_5-electrolyte system can be best revealed via in situ methods. Recently, various state-of-the-art in situ analysis methods have been utilized to uncover the structural changes in electrochemical interface of V_2O_5 electrodes such as in situ X-ray diffraction, in situ transmission electron microscopy, and in situ Raman.[9,14–16] Among them, in situ spectroscopic Raman detection is a powerful and sensitive tool to understand local structural variations of the electrode-electrolyte interface for the complex electrochemical interactions during cycling. A notable example is in situ spectroscopic Raman

Z. Zhang, W. Xie, J. Li, H. Zhang, J. Gao, H. Cao
Laboratory of Advanced Nano Materials and Devices
Ningbo Institute of Materials Technology and Engineering
Chinese Academy of Sciences
Ningbo 315201, China
E-mail: zhanghl@nimte.ac.cn; h_cao@nimte.ac.cn
Z. Zhang
Nano Science and Technology Institute
University of Science and Technology of China
Suzhou 215123, China
H. Zhang, H. Cao
Center of Materials Science and Optoelectronics Engineering
University of Chinese Academy of Sciences
Beijing 100049, China
Q. Wang, C. Zhang, G. Xu
Ningbo Wakan Electronic Science Technology Co. LTD
Ningbo 315475, China
A. A. Rogachev
Optical anisotropic films laboratory
Institute of Chemistry of New Materials of the National
Academy of Sciences of Belarus
Minsk 220141, Belarus
The ORCID identification number(s) for the author(s) of this article can be found under https://doi.org/10.1002/admi.202200883.

DOI: 10.1002/admi.202200883

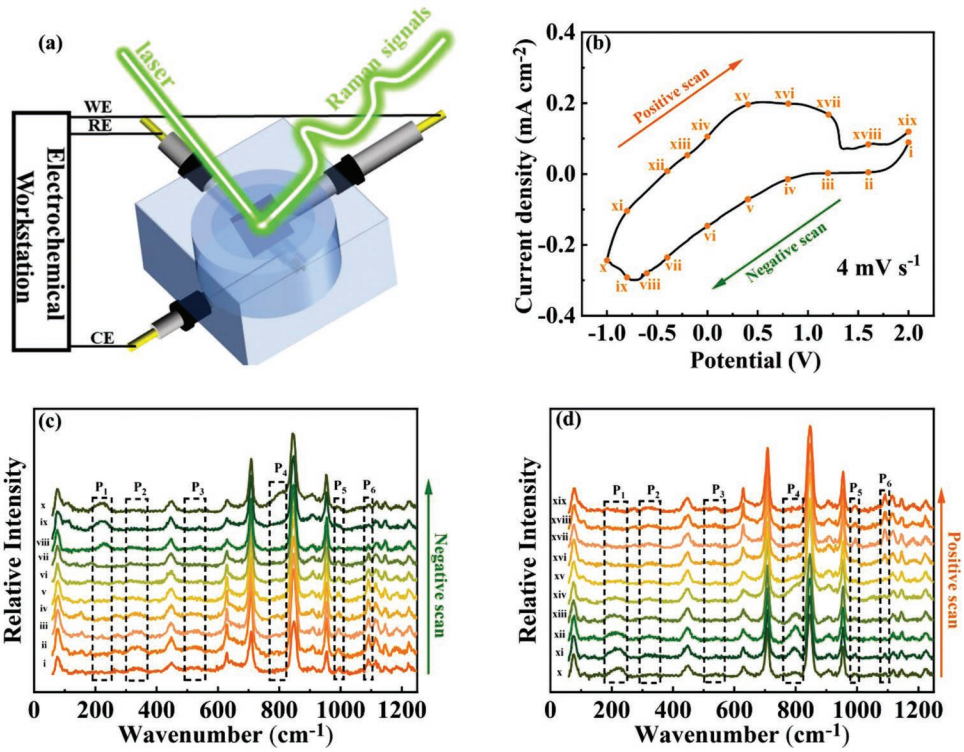

Figure 1. a) Schematic diagram of the in situ Raman Characterization under a three-electrode mode. b) CV curves of the V_2O_5 thin film in 0.1 M PC-$LiClO_4$ solution at the scan rate of 4 mV s^{-1}. In situ Raman spectra of V_2O_5 thin film during CV process in c) negative-going and d) positive-going sweeps.

characterization of lithium intercalation and deintercalation in thin film Li-ion battery electrodes to monitor the microstructural evolution of the Li—V—O system, which indicates fully reversible structural changes from the α- to δ-phase, irreversible γ-phase with the permanent bond breaking, and weakly crystallized ω-phase.[17] In terms of nanocrystal-in-glass V_2O_5 thin films, we have proposed ex situ Raman spectroscopic analysis to identify a distinct difference of three vibrational modes of —O—V—O—V—O—, V—O_3 bending, and V—O stretching between colored and bleached states in our previous work.[10] Although such ex situ Raman spectroscopic characterization of the V_2O_5 thin films has been widely considered, designing in situ strategy to uncover the dynamically structural transformation of nanocrystal-in-glass V_2O_5 electrode in real-time during its electrochemical lithium intercalation and deintercalation still needs to be experimentally explored further.

In this work, the Raman spectroscopy combined with cyclic voltammetry (CV) method in an electrochemical cell was performed to probe dynamically structural transformation induced by electrochemical lithium intercalation and deintercalation from the V_2O_5 thin films. Combining in situ Raman and UV-vis spectroscopy allows for the reversible structural transformation of V—O, V_3—O, and V—O bonds and reversible redox from V_2O_5 to lithium vanadate ($Li_xV_2O_5$) to be identified for the multi-electrochromic V_2O_5 thin films with a superior optical modulation of 75.41%.

2. Results and Discussion

To dynamically investigate ion transfers at the electrode-electrolyte interface, in situ Raman characterization coupled with CV measurements were performed in three-electrode cells. **Figure 1**a shows the schematic diagram of an in situ Raman measurement system, where WE, CE, and RE refer to the working electrode, counter electrode, and reference electrode, respectively. Figure 1c,d respectively exhibit the in situ Raman spectra of the V_2O_5 films during the negative-going and the positive-going sweeps, which is monitored by the CV (Figure 1b) in 0.1 M lithium perchlorate-propylene carbonate ($LiClO_4$-PC) solution at the scan rate of 4 mV s^{-1}. The potential sweep started from +2.0 V in a negative-going sweep and then swept back at −1.0 V in the positive-going sweep. As shown in Figure 1c,d, the broad, low-intensity Raman peaks compared to the classic Raman spectra of crystalline V_2O_5 indicate that the Raman response arises from the amorphous state of the V_2O_5 thin film,[18] as confirmed in a previous report.[10] The broad band at 300–350 cm^{-1} (P_2) is associated with the vibration mode of the interchain V_3–O bond.[13,19] And the broadband at 530 cm^{-1} (P_3) can be traced to the stretching vibration mode of the intra V_3–O bonds in a V_2O_5 unit cell.[12] There are two broad peaks at around 223 (P_1) and 800 cm^{-1} (P_4), which are related to the valence changes in vanadium ions (between V^{3+} and V^{4+}).[20–22] The peaks located at 994 cm^{-1} (P_5) and 1090 cm^{-1} (P_6) can be identified as the V–O and V–O bonds stretching vibration mode, respectively.[11,23]

Figure 2 gives the detailed evolution of the in situ Raman spectra measured at various potentials during CV process. As shown in Figure 2a, the intensity of broad peaks at 300–350 cm^{-1} (P_2) and 530 cm^{-1} (P_3) significantly decreases in reduction process (i-x, disappear at "v") and then increases to the original state in oxidation process (x-xix, appear at "xvi"), underscoring the reversible alteration of V_3–O bonding character and disorder

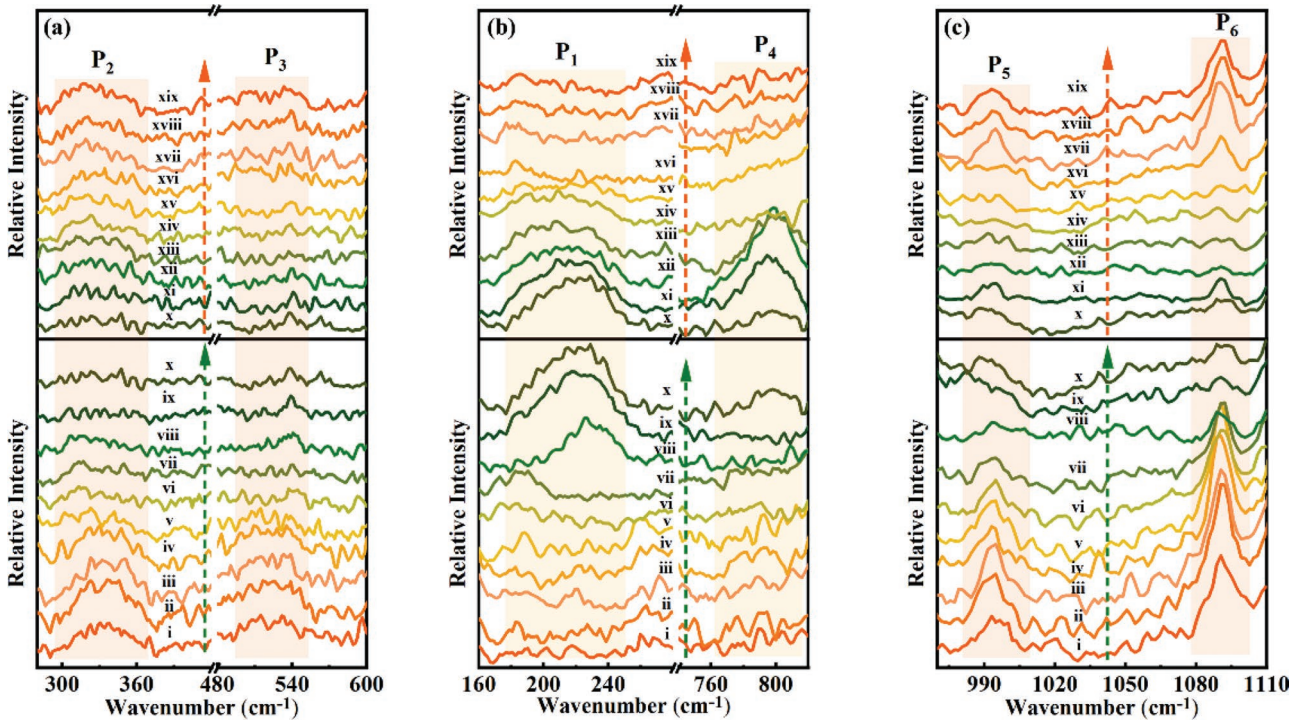

Figure 2. Enlarged view of the in situ Raman spectra at peak a) P_2 or P_3, b) P_1 or P_4, and c) P_5 or P_6 during the cycling process.

degree in the V_2O_5 film during the electrochemical process, which can be due to the reversible intercalation/deintercalation of lithium ions into/from the V_2O_5 thin film. For Figure 2b, the intensity of two new broad peaks located at around 223 (P_1) and 800 cm^{-1} (P_4) enhances greatly in the negative-going sweep (i-x) and then completely disappear when the potential reaches the first oxidation peak (xvi) in CV process. The result can be attributed to the reversible redox transition of vanadium ions (according to the reaction equation[1]: $V_2O_5 + xLi^+ + xe \leftrightarrow Li_xV_2O_5$) caused by the reversible insertion/extraction of lithium ions.[1,20–22] Figure 2c shows that the intensity of Raman spectra at 994 cm^{-1} (P_5) and 1090 cm^{-1} (P_6) diminishes substantially when the potential tends to be more negative (i-x), which results from an increase of disorder within the V_2O_5 thin film and a fairly sharp weakening of the V–O and V–O bonds at deep insertion of lithium ions.[12] Moreover, the intensity of peaks assignment at 994 cm^{-1} (P_5) and 1090 cm^{-1}(P_6) grows from the first oxidation peak (xvi) and recovers to the original level after the potential reaches the second oxidation peak (xvii) in the positive-going sweep during CV process, indicating the reversible extraction of lithium ions from the V_2O_5 thin film. In fact, the intercalation and de-intercalation of lithium ions in the V_2O_5 thin film can be further supported by the X-ray photoelectron spectra (XPS) results (Figure S1, Supporting Information). An estimation of $Li_{1.96}V_2O_5$ (Table S2, Supporting Information) at a typical colored voltage (–1.0 V) is confirmed, indicating intercalation of lithium ions. No distinct difference of Li_{1s} component in the V_2O_5 thin films between the typical bleached state (+2.0 V) and the as-deposited state is observed. In other words, Li_{1s} component with a content close to 0 (Table S2, Supporting Information) confirms that the intercalated Li ions were de-intercalated from the V_2O_5 thin films driven by the positively bleached state (+2.0 V).

For further understanding of the kinetic process of lithium-ions diffusion, the CV curves of the V_2O_5 thin film were tested at various scan rates from 2 to 10 mV s^{-1} in the 0.1 M $LiClO_4$-PC solution. As shown in **Figure 3**a, all the curves exhibit a similar shape, revealing the reversibility of the V_2O_5 electrode.[24] The dynamic behavior of lithium ions during electrochemical process can be further investigated according to the diffusion coefficients (D) calculated by the peak current (i) and scan rate (v),[25] as shown in Figure 3b. Apparently, the diffusion coefficient of reduction peak is about 2.5 and 1.2 times larger than that of oxidation peak 1 and 2, respectively, suggesting that intercalation is easier than deintercalation for lithium ions. The most plausible explanation can be concluded that the intercalation of lithium ions into the V_2O_5 thin film during the reduction process leads to the transformation from a semiconductor (V_2O_5) to a conductor ($Li_xV_2O_5$),[8] and thus the V_2O_5 thin film in the reduced state exhibits faster ion transfer kinetic compared to the V_2O_5 thin film in the oxidized state.[26] Furthermore, the diffusive effect of lithium ions at different redox peaks can be characterized by the following Equation (1)[27]

$$i = a^v b \tag{1}$$

where a and b (the slope of the "log v – log i" line) are parameters, i and v are the peak current and scan rate in CV curves, respectively. Commonly, the diffusion behavior and capacitive behavior (pseudo-capacitance and electric double layer capacitance) dominate the redox process respectively when the b-value approaches 0.5 and 1.0.[24,28] As shown in Figure 3c, the value of b in reduction state is determined to be 0.63, indicating the coexistence of the diffusion behavior of lithium ions intercalation into the V_2O_5 thin film and the capacitive behavior.[28]

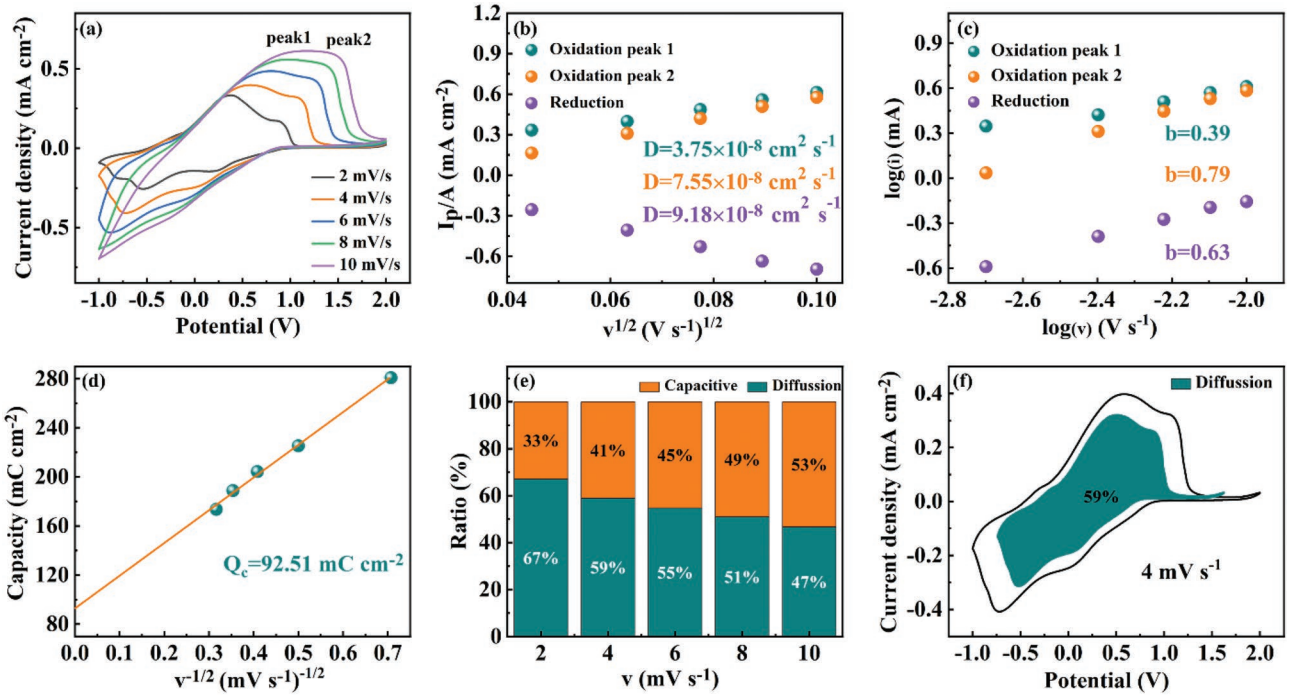

Figure 3. a) CV curves of the V_2O_5 thin film in 0.1 M PC-$LiClO_4$ solution at the scan rates of 2, 4, 6, 8, and 10 mV s^{-1}, respectively. b) the relationship between the peak current densities (I_p) and the square root of scan rate ($v^{1/2}$) and c) power law dependence of the peak current versus the scan rate for theV_2O_5 thin film in 0.1 M PC-$LiClO_4$ solution at oxidation (peak 1 and peak 2) and reduction states. d) Capacitive capacity. e) The contribution of diffusion-controlled behavior at different scan rates of the V_2O_5 thin film. f) Diffusion storage (blue) corresponding ratio at 4 mV s^{-1}.

The values of *b* at peak 1 and 2 during oxidation process are respectively calculated to be 0.39 and 0.79, revealing that the measured current in the first oxidation peak is primarily due to the diffusion of lithium ions extraction, and the ratio of capacitive behavior increases at the second oxidation peak. Most of the lithium ions intercalated in the V_2O_5 thin film during the reduction process are extracted after the first oxidation peak. As mentioned above, the Raman peak intensities of the VO bonds return to the initial level after the first oxidation peak during CV process due to the extraction of the lithium ions.

In addition, the contribution of diffusion behavior to the total charge in the CV curve can be determined by the following Equation (2)[29]

$$Q_{(v)} = Q_c + k \times \boldsymbol{v}^{-1/2} \quad (2)$$

where *k* is a parameter, Q(*v*) is the total charge storage, Q_c and $k \times v^{-1/2}$ respectively present the capacitive charge and diffusion-controlled charge. And Q_c is the capacitive charge when the scan rate (*v*) tends to infinity (Figure 3d). The calculated result in Figure 3e indicates that the diffusion-contributed ratio decreased from 67% at 2 mV s^{-1} to 47% at 10 mV s^{-1}, originating from the shortened diffusion time of lithium ions.[30] Figure 3f can be obtained by defining the relationship between $v^{1/2}$ and $i/v^{1/2}$ (Detailed calculation and figure (Figure S2, Supporting Information) are given in the Supporting Information),[31] showing that 59% of the total charge storage of the V_2O_5 thin film at 4 mV s^{-1} is derived from the diffusion behavior of lithium ions.

Figure 4a illustrates a series of in situ transmittance spectra by applying various potentials in the wavelength range of 300–850 nm to investigate the electrochromic performance of the V_2O_5 thin film. The bleached V_2O_5 thin film at +2.0 V shows a higher optical transmittance compared with the as-deposited V_2O_5 thin films. Compared with the as-deposited state, the V^{5+} proportion of the bleached V_2O_5 thin film obviously increases from 75.91% to 81.15%, and correspondingly V^{4+} decrease from 18.01% to 10.78% (Table S1, Supporting Information). It is reported that the concentration of free carriers in the film decreases with the increase of the proportion of high-valent vanadium (V^{5+}).[32] Consequently, the film can change from the strong absorption characteristics of metalloids to the weak absorption characteristics of oxide-like films, and consequently the refractive index and extinction coefficient decrease.[33] Thus, the bleached V_2O_5 thin film at +2.0 V shows a higher optical transmittance at λ = 800 nm compared with the as-deposited V_2O_5 thin film. The V_2O_5 thin film displays a superior optical modulation (ΔT) of 75.41% at λ = 800 nm than V_2O_5-based thin films on ITO/PET (67.01% at 700 nm), FTO/glass (50% at 780 nm), and ITO/glass (42.6% at 800 nm) substrates.[1,8,34] The outstanding optical modulation capability of the V_2O_5 thin films on ITO/Ag/AZO/PET (IAA/PET) substrate can be explained as follows. On one hand, the higher refractive index of IAA sandwich structures relative to ITO results in an excellent antireflection effect of the V_2O_5/IAA/PET thin films,[35] which enables the V_2O_5 thin films to obtain a transmittance of up to 93.89% in the bleached state. On the other hand, the deepening of the colored state can be attributed to the low resistance of the IAA

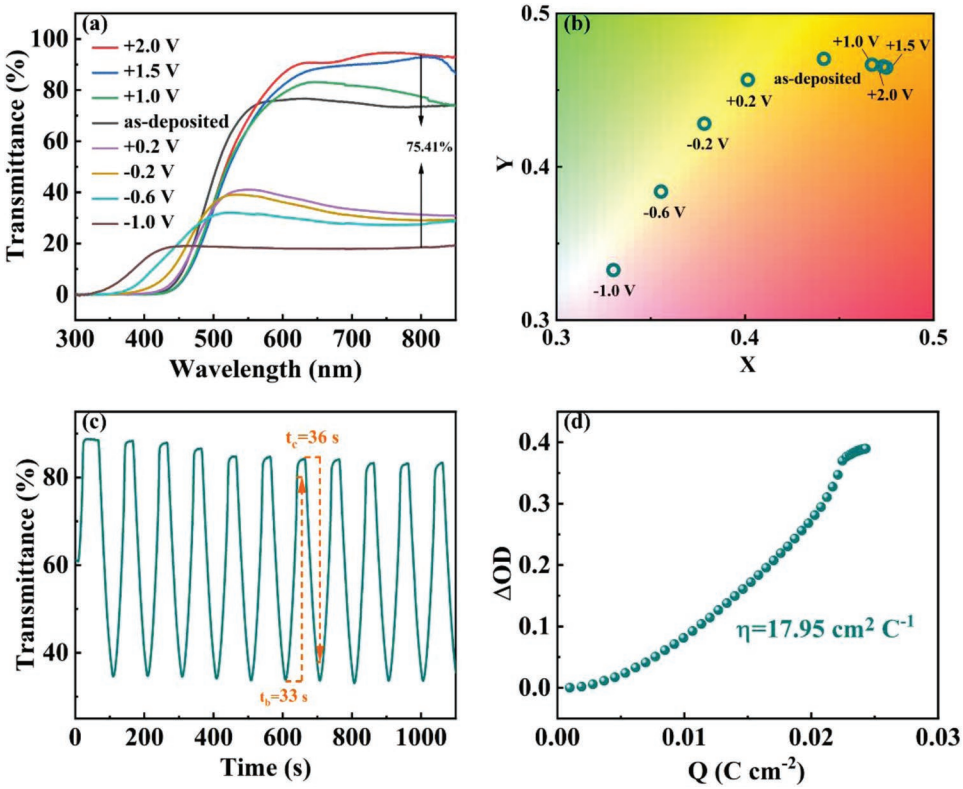

Figure 4. a) In situ transmittance spectrum of the V_2O_5 thin films at different constant potentials of +2.0 V, +1.5 V, +1.0 V, +0.2 V, −0.2 V, −0.6 V, and −1.0 V. b) CIE color coordinates of the V_2O_5 thin film under different color states. c) Switching time and in situ transmittance spectrum at $\lambda = 800$ nm (−1.0 V/+2.0 V, 100 s per cycle). d) Variation of the optical density (ΔOD) and charge density (Q) at $\lambda = 800$ nm.

substrate that can reduce the obstacle of lithium ions diffusion at electrode-electrolyte interface, providing greater opportunities for more lithium ions intercalation into the V_2O_5 thin film. Besides, the cross-sectional image of the V_2O_5 thin film (Figure S4, Supporting Information) confirms that the V_2O_5 thin film possesses a multilayered characteristic, and the thickness of the thin film is estimated to be ≈2.82 µm. It is well-known that the layered structure of the V_2O_5 thin films facilitates the intercalation of lithium ions,[10,36] and the optical contrast increases with increasing film thickness within a certain range of film thickness.[37,38] In fact, on the basis of the aforementioned in situ Raman results, the obvious reversible transformation from V_2O_5 to $Li_xV_2O_5$ caused by the intercalation and deintercalation of lithium ions can contribute to reversible high optical transmittance change of the V_2O_5 thin films. It is well known that the color change of the V_2O_5 thin films is caused by the reversible intercalation and deintercalation of lithium ions.[39] Also, to further understand the change of $V_2O_5/Li_xV_2O_5$ and the electrochromic color change of the V_2O_5 thin film in the colored and bleached states, the lithium-to-vanadium (Li/V) atomic ratios calculated by considering the XPS peak areas were respectively found to be 1.96:2 for −1.0 V, 1.44:2 for −0.6 V, 0.82:2 for −0.2 V and 0.68:2 for +0.4 V, compared with the near-zero values of Li/V for +2.0 V and as-deposited state (Figure S5, Supporting Information). The values of x in various colored and bleached states can be summarized in Table S2, Supporting Information. The digital photographs of the flexible V_2O_5 thin films at different states are shown in Figure S6, Supporting Information. In addition, Figure 4b exhibits their enlarged CIE 1931 chromaticity coordinates with an X range from 0.33 to 0.47 ((x, y) values are listed in Table S3, Supporting Information). The V_2O_5 thin films display multi-color changes from blackish-green to reddish-orange due to the intercalation and deintercalation of lithium ions in the voltage range of −1.0 V to +2.0 V. As Figure 4c shows, the colored and bleached switching times of the V_2O_5 thin film, which is stipulated the time required for the change in transmittance of the film to reach 90% between the colored and bleached states, are respectively calculated to be 36 s and 33 s in the in situ optical transmittance spectra at $\lambda = 800$ nm. In addition, the coloration efficiency (η), which is defined as the change in optical density (ΔOD) caused by the charge stored per unit area of the V_2O_5 thin film at a specific wavelength during the coloration process, can be calculated by the following standard Equation (3)[40]

$$\eta = \Delta OD/q = \log\left(T_{\text{bleached}}/T_{\text{colored}}\right)/q \quad (3)$$

where T_{bleached} and T_{colored} respectively denote the transmittance of the V_2O_5 thin film in bleached and colored states. The value of coloration efficiency of the V_2O_5 thin film is estimated to be 17.95 $cm^2\ C^{-1}$ at 800 nm, as shown in Figure 4d.

As revealed in **Figure 5**, the electrochemical impedance spectroscopy (EIS) was carried out to investigate the electrochemical behavior and interfacial properties of the V_2O_5 thin film at different potentials with a signal amplitude of 10 mV over a frequency range of 100 mHz-100 kHz. Figure 5a–c depict the

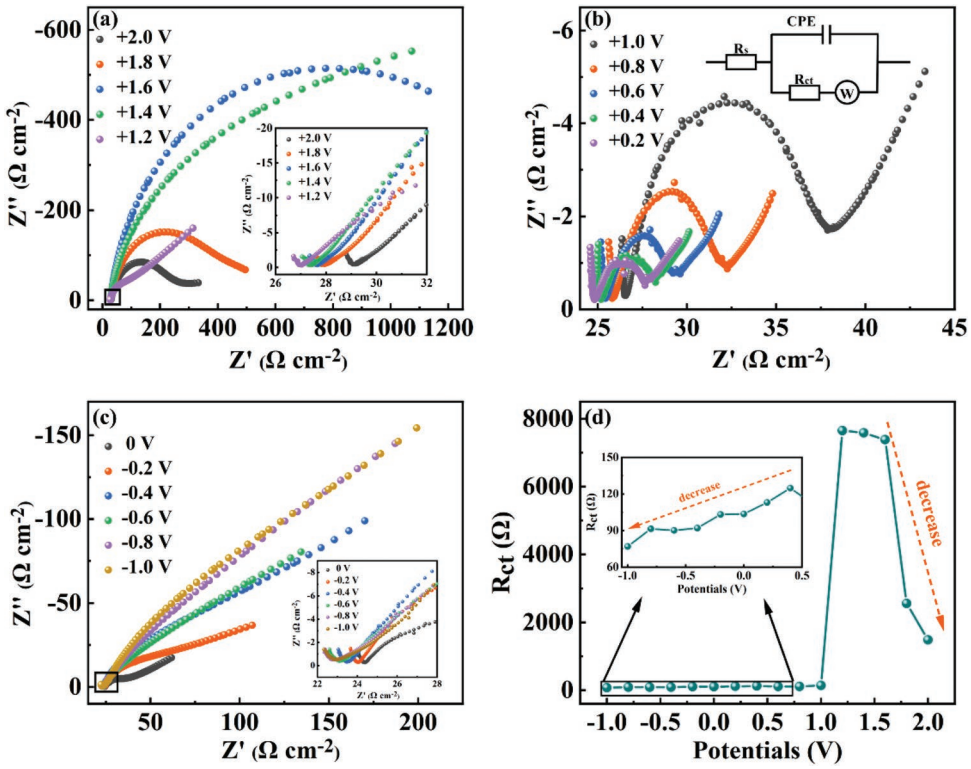

Figure 5. a,b, c) Nyquist plots of the V_2O_5 thin film at various constant potentials, the insets show the enlarged Nyquist plots in the high-frequency region (a and c) and equivalent circuit model (b), respectively. d) The fitted results of interfacial charge transfer resistance (R_s).

Nyquist plots of the V_2O_5 thin film in the potential region –1.0 to +2.0 V. A semicircle part related to the charge transfer and an inclined line correlated with ions diffusion constitute the Nyquist plot.[41] The inset in Figure 5b presents the equivalent circuit used to fit the EIS spectra,[42] and detailed fit data are given in Table S4, Supporting Information The Warburg impedance, *W*, reflects the diffusion kinetics of lithium ions in the V_2O_5 thin films.[43] R_{ct} is the interfacial charge transfer resistance at the electrode-electrolyte interface, which can be defined as the semicircle diameter at high frequency of the Nyquist plots.[43] The electrolyte resistance (R_s) can be obtained from the intersection of the spectra with the real axis at high frequency of the Nyquist plots.[43,44] Figure 5d shows the variation of the fitted values of R_{ct} at different potentials. It is worth noting that the values of R_{ct} at negative bias voltages are much lower than that in forward bias voltages, from 76.97 to 7648 Ω, as listed in Table S4, Supporting Information. While the linear slopes in the low-frequency region negatively correlated with semi-infinite Warburg diffusion processes show the opposite variation trend.[1] As analysis of the in situ Raman above, under negative bias voltages, the intercalation of a large amount of lithium ions into the V_2O_5 thin film changes its VO bonding characteristic, resulting in the transformation of the V_2O_5 thin film from the semiconductor (V_2O_5) to the conductor ($Li_xV_2O_5$).[8] And the improvement of conductivity of the V_2O_5 thin film accelerates the migration of lithium-ion at electrode-electrolyte interface,[26,42,45] which is consistent with the above analysis of the diffusion coefficient (*D*) of lithium ions. Besides, the value of R_{ct} is greatly decreased with the increase of forward or negative bias potential, indicating that the electrochemical reaction proceeds more easily at high voltage.[46]

3. Conclusions

In summary, we develop and apply in situ spectroscopic methods combined with electrochemical techniques to relate the structure and performance evolution of the V_2O_5 thin films on the ITO/Ag/AZO/PET substrates to the behavior of lithium-ion intercalation and deintercalation. The in situ Raman spectroscopy and electrochemistry tests suggest that the reversible insertion/extraction of lithium ions can lead to the reversible transformation of the V_2O_5 thin films from V_2O_5 to $Li_xV_2O_5$. Furthermore, the vibrational modes of V–O, V_3–O, and V–O bonds can be Raman active and silent reversibly induced by the reversible insertion/extraction of lithium ions. The optical transmittance spectra combining with direct in situ Raman evidences demonstrate that the multi-color electrochromic characteristic with a superior optical modulation of 75.41% can be benefited from both the reversible $V_2O_5/Li_xV_2O_5$ transformation and the reversible evolution of VO bonding characteristic. On the basis of the further electrochemical analyses and in situ Raman results, it is uncovered that the intercalation of lithium ions can convert the V_2O_5 thin films from a semiconductor (V_2O_5) to a conductor ($Li_xV_2O_5$), which facilitates the migration of lithium ions. This work deploys and provides a unique and more granular investigation approach for revealing the ion transfer kinetics

at electrochemical interface and the evolution of thin film performance with ion migration.

4. Experimental Section

Synthesis: The V_2O_5 thin films were prepared by two-electrode electrochemical deposition. The ITO (40 nm)/Ag (10 nm)/AZO (40 nm)/PET transparent flexible substrate was used as the working electrode and a platinum sheet was used as the counter electrode. The transmittance and sheet resistance of the ITO/Ag/AZO (IAA) thin film electrode are about 83% (at 550 nm) and 15 Ω sq^{-1}, respectively. Details of the experimental procedure have been reported elsewhere.[10] After electrodeposition, the absolute ethyl alcohol was used to rinse the loosely bounded particles on the surface of the V_2O_5 thin films. Finally, the samples were dried at 60 °C for 12 h in air.

Measurements: In situ Raman spectra were measured with a Renishaw inVia Reflex confocal microscopy Raman system (532 nm laser source) and an electrochemical workstation (CHI660D, Chen Hua Shanghai), where the Raman spectra were recorded one by one during a CV process (4 mV s^{-1}) in the potential range from –1.0 V to +2.0 V and were captured every 15 s. The chemical states and elements were analyzed by X-ray photoelectron spectra (XPS) (AXIS UTLTRA DLD). The morphological characteristic of the thin film was characterized by the field emission scanning electron microscope (FESEM, S4800). In situ optical spectroscopy measurements were performed using electrochemical workstation (CHI660D, Chen Hua Shanghai) and UV-vis spectroscopy (Perkin–Elmer Lambda 950). The electrochemical property experiments of V_2O_5 film were tested with an electrochemical workstation (CHI660D, Chen Hua Shanghai). CV measurements of the V_2O_5 thin films were carried out by a standard three-electrode system, where a platinum sheet served as the counter electrode, KCl saturated $Hg/HgCl_2$ as the reference electrode, and 0.1 M $LiClO_4$-PC solution as the electrolyte. The EIS were measured by utilizing an electrochemical workstation (Zennium, IM6) over a frequency range of 100 mHz–100 kHz.

Supporting Information

Supporting Information is available from the Wiley Online Library or from the author.

Acknowledgements

This project is supported by the National Natural Science Foundation of China (61974148) and Ningbo Science and Technology Innovation 2025 Major Special Project (2020Z002).

Conflict of Interest

The authors declare no conflict of interest.

Data Availability Statement

Research data are not shared.

Keywords

electrochromism, in situ Raman, structural transformation of nanocrystal-in-glass, vanadium pentoxide

Received: April 20, 2022
Revised: July 14, 2022
Published online: August 19, 2022

[1] L. Zhao, J. Kuang, W. Zhuang, J. Chao, W. Liao, X. Fu, C. Li, L. Ye, H. Liu, *Nanotechnology* **2021**, *33*, 054001.
[2] M. M. Potter, M. A. Yoder, A. Petronico, S. E. Lehman, B. G. Nicolau, M. J. Enright, M. Phelan, J. He, H. A. Atwater, R. G. Nuzzo, *ACS Appl. Energy Mater.* **2020**, *3*, 1540.
[3] H. Yu, M. Qi, J. Wang, Y. Yin, Y. He, H. Meng, W. Huang, *Electrochem. Commun.* **2019**, *102*, 31.
[4] Y. Wang, R. Shen, S. Wang, Q. Chen, C. Gu, W. Zhang, G. Yang, Q. Chen, Y.-M. Zhang, S. X.-A. Zhang, *Chem* **2021**, *7*, 1308.
[5] Y. Liu, C. Jia, Z. Wan, X. Weng, J. Xie, L. Deng, *Sol. Energy Mater. Sol. Cells* **2015**, *132*, 467.
[6] A. Ray, A. Roy, S. Bhattacharjee, S. Jana, C. K. Ghosh, C. Sinha, S. Das, *Electrochim. Acta* **2018**, *266*, 404.
[7] Y. Qi, K. Qin, Y. Zou, L. Lin, Z. Jian, W. Chen, *Appl. Surf. Sci.* **2020**, *514*, 145950.
[8] C. Wang, X. Zhang, S. Liu, H. Zhang, Q. Wang, C. Zhang, J. Gao, L. Liang, H. Cao, *ACS Appl. Energy Mater.* **2022**, *5*, 88.
[9] S. Deng, Y. Jiang, D. Huang, Z. Ma, C. Li, W. Xiao, X. Yan, *J. Alloys Compd.* **2022**, *891*, 161946.
[10] J. Wu, D. Qiu, H. Zhang, H. Cao, W. Wang, Z. Liu, T. Tian, L. Liang, J. Gao, F. Zhuge, *J. Electrochem. Soc.* **2018**, *165*, D183.
[11] D. Batyrbekuly, S. Cajoly, B. Laik, J. P. Pereira-Ramos, N. Emery, Z. Bakenov, R. Baddour-Hadjean, *ChemSusChem* **2020**, *13*, 724.
[12] A. Jarry, M. Walker, S. Theodoru, L. J. Brillson, G. W. Rubloff, *Chem. Mater.* **2020**, *32*, 7226.
[13] L. M. McGrath, J. F. Rohan, *Batteries Supercaps* **2021**, *4*, 485.
[14] P. Jing, W. Wei, W. Luo, X. Li, F. Xu, H. Li, M. Wei, D. Yu, Q. Zhu, G. Liu, *Inorg. Chem. Commun.* **2020**, *117*, 107953.
[15] J. Zhu, H. Shen, X. Shi, F. Yang, X. Hu, W. Zhou, H. Yang, M. Gu, *Anal. Chem.* **2019**, *91*, 11055.
[16] G. Zhang, T. Xiong, X. Pan, Y. Zhao, M. Yan, H. Zhang, B. Wu, K. Zhao, L. Mai, *Nano Res.* **2019**, *12*, 905.
[17] H. Jung, K. Gerasopoulos, A. A. Talin, R. Ghodssi, *Electrochim. Acta* **2017**, *242*, 227.
[18] K. L.e Van, H. Groult, A. Mantoux, L. Perrigaud, F. Lantelme, R. Lindstrom, R. Badour-Hadjean, S. Zanna, D. Lincot, *J. Power Sources* **2006**, *160*, 592.
[19] A. Jin, W. Chen, Q. Zhu, Y. Yang, V. L. Volkov, G. S. Zakharova, *Thin Solid Films* **2009**, *517*, 2023.
[20] C. Julien, G. A. Nazri, O. Bergström, *Phys. Status Solidi B* **1997**, *201*, 319.
[21] P. Shvets, O. Dikaya, K. Maksimova, A. Goikhman, *J. Raman Spectrosc.* **2019**, *50*, 1226.
[22] Y. Tutel, M. B. Durukan, S. Koc, S. Koylan, H. Cakmak, Y. Kocak, F. Hekmat, E. Ozensoy, E. Ozbay, Y. A. Udum, L. Toppare, H. E. Unalan, *J. Electrochem. Soc.* **2021**, *168*, 106511.
[23] Z. Bo, S. Qing, H. De-Yan, *Chin. Phys. B* **2009**, *18*, 4988.
[24] Q. Li, C. Xu, L. Yang, K. Pei, Y. Zhao, X. Liu, R. Che, *ACS Appl. Energy Mater.* **2020**, *3*, 7416.
[25] K. Wang, H. Zhang, G. Chen, T. Tian, K. Tao, L. Liang, J. Gao, H. Cao, *J. Alloys Compd.* **2021**, *861*, 158534.
[26] Z. Tong, J. Hao, K. Zhang, J. Zhao, B.-L. Su, Y. Li, *J. Mater. Chem. C* **2014**, *2*, 3651.
[27] E. Armstrong, D. McNulty, H. Geaney, C. O'Dwyer, *ACS Appl. Mater. Interfaces* **2015**, *7*, 27006.
[28] L.-Q. Yu, S.-X. Zhao, X. Wu, Q.-L. Wu, J.-W. Li, E.-L. Zhao, *CrystEngComm* **2019**, *21*, 6641.
[29] P. Yang, P. Sun, L. Du, Z. Liang, W. Xie, X. Cai, L. Huang, S. Tan, W. Mai, *J. Phys. Chem. C* **2015**, *119*, 16483.
[30] J. Wang, M. Sun, F. Wang, X. Zhang, J. Song, W. Zhang, M. Li, *Chem. Eng. J.* **2021**, *426*, 130895.
[31] S. Wang, H. Xu, T. Hao, P. Wang, X. Zhang, H. Zhang, J. Xue, J. Zhao, Y. Li, *NPG Asia Mater.* **2021**, *13*, 51.
[32] X. Dong, Y. Su, Z. Wu, X. Xu, Z. Xiang, Y. Shi, W. Chen, J. Dai, Z. Huang, T. Wang, Y. Jiang, *Appl. Surf. Sci.* **2021**, *562*, 150138.

[33] D. Xiang, W. Zhiming, J. Yadong, X. Xiangdong, Y. He, G. Deen, W. Tao, presented at *2014 SPIE 7th Symp. Adv. Opt. Manuf. Test. Technol. Optoelectron. Mater. Devices Sens. Imaging.*, Harbin **2014**.
[34] W. T. He, Y. N. Liu, Z. Q. Wan, C. Y. Jia, *RSC Adv.* **2016**, *6*, 68997.
[35] N. Ren, P. Shi, Z. Sheng, K. Zhong, H. Du, Q. Shan, J. Zhu, T. Li, S. Ban, *Sol. Energy* **2020**, *203*, 240.
[36] D. Qiu, J. Wu, L. Liang, H. Zhang, H. Cao, W. Yong, T. Tian, J. Gao, Z. Fei, *J. Nanosci. Nanotechnol.* **2018**, *18*, 7502.
[37] S. Surendren, B. Deb, *Electrochim. Acta* **2021**, *389*, 138629.
[38] Q. Shi, G. Zhang, Y. Wang, Y. Lan, J. Wang, G. Cheng, *Nanomaterials* **2021**, *11*, 2078.
[39] J.-L. Wang, J.-W. Liu, S.-Z. Sheng, Z. He, J. Gao, S.-H. Yu, *Nano Lett.* **2021**, *21*, 9203.
[40] S. Zhang, S. Chen, Y. Luo, B. Yan, Y. Gu, F. Yang, Y. Cao, *J. Alloys Compd.* **2020**, *842*, 155882.
[41] R. Narayanan, A. Dewan, D. Chakraborty, *RSC Adv.* **2018**, *8*, 8596.
[42] M. Sivakumar, M. Sakthivel, S.-M. Chen, V. Veeramani, W.-L. Chen, G. Bharath, R. Madhu, N. Miyamoto, *Ionics* **2017**, *23*, 2193.
[43] M. Panagopoulou, D. Vernardou, E. Koudoumas, N. Katsarakis, D. Tsoukalas, Y. S. Raptis, *J. Phys. Chem. C* **2017**, *121*, 70.
[44] R. S. Ingole, B. Y. Fugare, B. J. Lokhande, *AIP Conf. Proc.* **2016**, *1724*, 020080.
[45] Y. Zhang, X. Jing, Q. Wang, J. Zheng, H. Jiang, C. Meng, *Dalton Trans.* **2017**, *46*, 15048.
[46] H. Elbohy, A. Thapa, P. Poudel, N. Adhikary, S. Venkatesan, Q. Qiao, *Nano Energy* **2015**, *13*, 368.